CASE STUDY IN VALIDATING CAPILLARY PRESSURE CURVES, RELATIVE PERMEABILITY AND RESISTIVITY INDEX OF CARBONATES FROM X-RAY MICRO TOMOGRAPHY IMAGES

Zubair Kalam*, Taha Al Dayyani*, Andrew Clark*, Sven Roth[#], Cyril Nardi[#], Olivier Lopez[#], and Pål-Eric Øren[#]
* Abu Dhabi Company For Onshore Oil Operations (ADCO), Abu Dhabi, UAE
[#] Numerical Rocks AS, Stiklestadveien 1, 7041 Trondheim, Norway

This paper was prepared for presentation at the International Symposium of the Society of Core Analysts held in Halifax, Nova Scotia, Canada, 4-7 October, 2010

ABSTRACT

X-ray micro tomography combined with pore-scale modeling is one of the growth areas in reservoir core parameter evaluations. This technique has seen phenomenal growth in evaluating challenging parameters like relative permeability, formation resistivity, electrical resistivity (and hence resistivity index), capillary pressure and directional absolute permeability (k_x, k_y and k_z).

Reservoir cores, comprising three distinct rock types from a mature producing carbonate formation in Middle East, varying in permeability from micro-Darcy (0.02 mD) to several Darcy (5700 mD) were examined using X-ray microtomography. We present *e-Core* predictions for porosity, absolute permeability, formation resistivity factor, capillary pressure curves, water-oil relative permeability curves, and resistivity indices (saturation exponents 'n') for primary drainage and imbibition, respectively.

The results confirm the quick turnaround capability in reservoir parameter evaluations from X-ray micro tomography imaging. Required sample sizes and preparations, usually associated with conventional special core analysis (SCAL) techniques are minimized. Our results confirm the validity of this technique even on locally heterogeneous carbonates. The *e-Core* technology (Numerical Rocks' internal software) of pore network extraction and pore scale modeling is increasingly well established in being able to predict both single phase and two-phase flow properties in reservoir rocks.

INTRODUCTION

The main objective of this study is to numerically predict petrophysical properties, capillary pressure and relative permeability curves for carbonate rocks from rock models derived from X-ray micro tomography imaging (MCT). The traditional way to gather petrophysical information and flow parameters of reservoir rocks is to perform laboratory experiments. However, laboratory core analyses are time consuming and it is often difficult to achieve the desired wetting and saturation states, especially when dealing with

low porosity and low permeability carbonates (e.g. micritic limestones). Moreover, it can be destructive for the sample material. Unlike most reservoir sandstones, which typically contain a single intergranular pore system, the porosity distribution in carbonate rocks is more complex making evaluation of the rock types even more complicated.
Direct imaging of reservoir rocks via MCT is, next to process-based modelling (Bakke and Øren, 1997; Øren et al., 1998; Øren and Bakke, 2002), a promising approach that results in a three-dimensional representation of the rock framework and the pore network, and allows numerical computations of petrophysical properties and fluid flow properties.
In this study three different rock types from a producing Lower Cretaceous Middle East carbonate formation were digitally reconstructed using the MCT approach. Single–phase petrophysical properties, such as porosity, absolute permeability, mercury injection capillary pressures (MICP), and formation resistivity factors (FRF) were directly calculated on the grid-based MCT models. Capillary pressure curves, relative permeability curves (kr) and resistivity indices (RI) for primary drainage, water flooding, and secondary drainage were simulated on a pore-network representation of the MCT models. The appropriateness of the predicted properties is tested by comparing the results with laboratory derived data sets.

MATERIAL AND METHODS

Characterization of The Reservoir Core Samples

Sample Sn-5

Sample Sn-5 is a 1.5" cylindrical horizontal core plug drilled from a vertical conventional core, consisting of mainly Lower Cretaceous coated-grain, skeletal grainstone (CgSG Fig. 1). The sample depth is 8231.83 feet (MD). This lithofacies is interpreted to represent deposition in a shallow carbonate sub-tidal, high energy open platform, upper ramp, near a shoal crest (Strohmenger et al., 2006). Sample Sn-5 has an ambient helium porosity of 26.8 % and gas permeability of 5663mD.
The porosity, permeability and MICP results indicate that this sample belongs to “rock type 1” (RRT-1), according to one of ADCO’s recent carbonate reservoir rock-typing definitions (Grotsch, 1997). This rock type designation implies a porosity of >14% and permeability of > 500 mD.

Sample Sn-34

Sample Sn-34 is a 1.5" cylindrical horizontal core plug drilled from a vertical conventional core, consisting of mainly Lower Cretaceous Skeletal, Peloid Packstone (SPP; Fig. 2). The sample depth is 8270.17 feet (MD). This lithofacies is interpreted to represent deposition in a shallow sub-tidal to inter-tidal, moderate-energy restricted platform, inner shoal and upper ramp.
The sample has a measured ambient helium porosity of 22.6 % and gas permeability of 2.92 mD, implying this sample belongs to “RRT-5”, according to the previously mentioned ADCO scheme.

Sample Sn-40

Sample Sn-40 is a 1.5" cylindrical horizontal core plug drilled from a vertical conventional core, consisting of mainly Lower Cretaceous skeletal, peloid wackestone-packstone (SPWP; Fig. 3). The sample depth is 8276.83 feet (MD). This lithofacies is interpreted to represent deposition in a sub-tidal, low-energy open platform, upper to middle ramp environment, near the fair weather base. This sample had an ambient helium porosity of 11.2 % and gas permeability of 0.02 mD, implying that this sample belongs to "RRT-7".

X-ray Micro-tomography And Data Processing

X-ray micro-tomography allows the 3D imaging of rock samples down to sub-micron resolutions. It is a non-destructive technique. The MCT measurements were performed in the European Synchrotron Radiation Facility (ESRF, Grenoble, France) using the ID19 beamline and a FReLoN 2048x2048 pixel camera as detector. During the data acquisition, about 1500 radiographs are recorded, while the sample is rotating from 0 to 180°. A series of 2D slices is then reconstructed (standard filtered back-projection), which are stacked together to build a 3D image (Boller, 2006).

The grain stone sample Sn-5 was imaged with a voxel size of 7.39µm; the micritic samples Sn-34 and Sn-40 were imaged with voxel sizes of 0.28µm. The low porosity sample Sn-40 showed extremely fine pore structures. Therefore, the voxel resolution was artificially doubled by interpolating the grey values of the neighbouring voxels, which resulted in a voxel size of 0.14µm. The grain stone Sn-5 MCT was sub-sampled into a 900x900x700 voxel volume corresponding to 6.7 x 6.7 x 5.2 mm side lengths. Sn-34 and Sn-40 were sub-sampled into 1000^3 voxel volumes corresponding to a physical size of 280x280x280µm and 140x140x140µm for Sn-34 and Sn-40, respectively.

In order to remove artefacts and enhance the data quality the cubes were filtered using a smallest-univalue-segment-assimilating-nucleus filter (SUSAN filter; http://www.pvv.org/~perchrh/imagej/smooth.html). Consequently, the MCT volumes were segmented into the solid phase and the pore space, resulting in digital, grid-based MCT models containing the pore-space information of the original rocks.

Petrophysical Parameters

While the porosity results from the imaging and segmentation process, absolute permeabilities, formation resistivity factors and MICP simulations were directly calculated on the grid-based MCT models. Permeabilities are computed by solving the Navier-Stokes equation, the formation factors are computed by solving a Laplacian equation as previously reported by Øren and Bakke (2002). Absolute permeabilities and formation factors were calculated in all directions (x-, y-, z-dir) on the MCT models for the individual samples.

Two-phase Flow Simulations
Simulation of multiphase flow requires the extraction of a numerical pore network, which retains the essential features of the rock model's pore space (Dong and Blunt, 2009). The multi-phase flow simulations are based on a quasi-static network model. In the numerical simulations, flow is assumed to be capillary driven, fluids are immiscible and viscous forces are neglected (Bakke and Øren 1997; Øren et al., 1998). The wettability model used for the two-phase flow simulations is discussed in detail in Øren et al. (1998). The data points obtained from the water-oil two-phase flow simulations were fitted by the LET-correlation for the relative permeabilities (Lomeland et al., 2005) and the Skjaevelands correlation for the capillary pressure curves (Skjaeveland et al., 2000). The input data used for all flow simulations are summarized in Table 1.

Laboratory Measurements
Laboratory measurements for water-oil relative permeability during first imbibition and secondary drainage were available for the rock types corresponding to samples Sn-5 and Sn-34. Experiments on rock type of sample Sn-40 (which had micro-Darcy permeability) were very difficult and did not lead to satisfactory SCAL results. The laboratory experiments for rock types representative of Sn-5 and Sn-34 were carried out at commercial SCAL laboratories. The unsteady state and steady state water-oil experiments were performed at reservoir conditions with live-oil and synthetic formation water; data reported here were based on the steady state tests. The irreducible water saturation (Swi) was determined using the porous plate method fitted with in situ saturation monitoring. The SCAL samples were carefully selected to ensure representativeness of reservoir behaviour.

Porous Plates at reservoir temperature and reservoir overburden pressures were used to derive the representative laboratory evaluated saturation exponent 'n' and capillary pressure 'Pc', and in some cases these were supplemented with multi-speed and single-speed centrifuge measurements at 70 degrees Celsius.

RESULTS AND DISCUSSION

Sample Sn-5
Sn-5 Calculated Properties Versus Laboratory Measurements
The single-phase petrophysical properties are calculated dircetly on the grid-based MCT models. The calculated versus the laboratory petrophysical properties are summarized in Table 2a. The laboratory porosity measurement resulted in 26.8%, while the MCT model shows only porosity of approximately 19%. Thin section examination of this bioclastic grainstone indicated a considerable amount of microporosity. The rock is also made up of large bioclasts up to several hundreds of μm in diameter. In order to grasp the pore system that carries the main flow the imaged volume has to be big enough to build a representative elementary volume (REV). The size of the REV is directly dependent on the size of the rock constituents. For this rock type the physical volume (REV) should have side lengths of approximately five to six mm (estimated from grain measurements using a reflected-light microscope). Moreover, for computational reasons, the voxel size

of MCT images should currently not exceed 1000^3 voxel (extension of this restriction to 2000^3 voxel is currently in the focus of research). Honouring the above-mentioned requirements a voxel size of 7.4 µm was chosen for imaging. With this voxel size the REV for this rock could be reached. However, the large size of the volume that had to be imaged to obtain the REV (and at the same time keeping the image sizes computational manageable) leads to the loss of micron and sub-micron information; i.e. everything that is smaller than the imaging resolution of 7.4 µm cannot be resolved.

The "resolution-versus-volume issue" is a general challenge in all computational operations that deal with pixel/voxel images and is a pure computer hardware restriction.
The close match of the absolute permeability calculated on the MCT model with the laboratory measurements shows that the pore system carrying the main flow is well captured with the imaging parameters chosen (see Table 2a). In turn, the unresolved - but conductive - microporosity of the MCT model is mirrored in the higher formation factor with respect to the laboratory measurements. Capturing the main pore system builds the basis for the extraction of the simplified pore network and consequent two-phase flow simulations.

Sn-5 Results Of Two-phase Water-oil Simulations Versus Laboratory Experiments

Prior to the two-phase flow simulations a simplified numerical pore network was extracted (Bakke and Øren, 1997). The main simplification lies in the definition of the pore geometries, which are characterized by a shape factor describing round, quadratic, and triangular pore geometries. The simulations on sample Sn-5 have been performed assuming a mixed-wet rock. Table 2b gives the comparison between simulated data and laboratory data for n-exponents during primary drainage and first imbibition cycles and end-point saturations for imbibition and secondary drainage.

Generally, the data show a good correspondence with the exception of the irreducible water saturation (Swi) and the water relative permeability at residual oil saturation (krw @ Sorw). The former is related to the missing microporosity in the MCT model (which would increase the Swi); the latter is due to the laboratory set-up. The laboratory measurements show a krw value larger than one at Sorw, which might be related to uncertainties encountered during the laboratory experiments (e.g.: kro @ Swi is distinctly different from kabs). In the region of spontaneous imbibition only the numerical model provides data points and thus, no direct comparison can be made. All the different methods, laboratory and simulations performed on the MCT models, showed the same trend in the forced imbibition area ($Pc < 0$). This corroborates the finding that the main pore system has been successfully captured.

Figure 6a presents the comparison of simulated relative permeability curves versus laboratory measurements for water flooding. The comparison shows a slight discrepancy between the numerical results and the laboratory results, especially for the water relative permeability. This can be explained by the fact that in the laboratory experiments the krw @ Sorw is larger than 1. More investigation about relative permeabilities above one in

the laboratory experiments is needed in order to provide a more sophisticated comparison between numerical and laboratory derived data.

Figure 6b shows simulated relative permeability curves for secondary drainage versus laboratory measurements. As mentioned above, the krw @ Sorw from the laboratory measurements equals 1.22. The starting points are different and might affect the entire set of data. However, one can notice that in both cases water is trapped in the system, which is a good indication for the wettability of the rock. The "water trapping" is more pronounced in the laboratory measurement. The steeper slope of the kro curve at low water saturations, together with lower Sorw and lower final water saturation than the experiments indicate that the rock might have a more oil-wet behavior than simulated.

Sample Sn-34

Sn-34 Calculated Properties Versus Laboratory Measurements

The single-phase petrophysical properties are calculated directly on the grid-based MCT models. Calculated versus the laboratory petrophysical properties are summarized in Table 3a. The sub-sample extracted for MCT analysis shows approximately 3.9% higher porosity than the laboratory measurements. The higher porosity translates into the higher permeability of 6 mD simulated on the MCT model versus 2.92 mD in the laboratory measurement. The formation factor and calculated m-exponent are in exceptionally close agreement.

Sn-34 Results Of Two-phase Water-oil Simulations Versus Laboratory Experiments

Following the pore-network extraction the simulations on Sn-34 have been performed assuming a mixed-wet rock. Table 3b gives the comparison between simulated data and laboratory data for n-exponents during primary drainage and first imbibition and end-state saturations for imbibition and secondary drainage.

The results for saturation exponent 'n' during both primary drainage and imbibition are slightly lower for the *e-Core* simulations compared to the laboratory measurements. There is excellent consistency in the end point krw as well as the derived Swi and Sorw.
Figure 7a compares the results of the J-functions of the laboratory experiments and the numerical simulation performed on the MCT models. As mentioned for sample Sn-5, direct comparison can only be made in the region of forced imbibition where laboratory and numerical modeling provide data points. It is noted that the x-axis crossing point (Pc=0) occurs for a lower Sw during the laboratory experiments compared to the numerical results, indicating that the numerical model is simulated less oil-wet than the experiments show. However, the residual oil saturation value is in close match to the laboratory measurements. The more oil-wet character of the sample is corroborated by the difference in the final water saturations: 5% in the simulations versus 8 % in the experiments.

Figures 7b and 7c show the relative permeability curves for imbibition and secondary drainage for sample Sn-34. As for Sn-5, the laboratory measurements show a krw value larger than one at Sorw, which might be related to uncertainties encountered during the

laboratory experiments (e.g.: kro @ Swi is distinctly different from kabs). Despite this, the numerical and measured relative permeabilities are following the same trend and end point saturations are very close. The results are very encouraging, both in terms of relative permeabilities and capillary pressure perspectives.

Sample Sn-40

Sn-40 Calculated Properties Versus Laboratory Measurements

The single-phase petrophysical properties are calculated directly on the grid-based MCT models. The calculated versus the laboratory petrophysical properties are summarized in Table 4a.

The sub-sample extracted for MCT analysis shows approximately 3% higher porosity than the laboratory measurements. The higher porosity translates into a higher permeability, which is around 0.42 mD simulated on the MCT model versus 0.02 mD in the laboratory measurement. The formation factor is high, and consistent with the very high tortuosity calculated for the sample (7.21) unlike samples S-5 and Sn-34, which had tortuosity values in the range of 4.11 to 4.32, respectively. The calculated m-exponent is in close agreement to lab measurement.

Sn-40 Results Of Two-phase Water-oil Simulations Versus Laboratory Experiments

Following the pore-network extraction, the simulations on Sn-40 have been performed assuming water-wet conditions. Table 4b gives the comparison between simulated data and laboratory data for n-exponents and end-state saturations for imbibition and secondary drainage. The high n-exponent for D1 shows that the water gets very quickly disconnected during the drainage process suggesting that the smallest pores are not captured by the MCT model. This is commensurate with the high FRF (see Table 4a). It should be noted that no laboratory measurements of water-oil kr were possible due to the extremely low permeability of the samples of this rock type. The end points measured compared well with the MCT models, and thus enhance the validity of the *e-Core* technology.

Figure 8a shows the results of the J-function of the numerical simulation on the MCT model. Figures 8b and 8c show the simulated relative permeability curves for imbibition and secondary drainage for sample Sn-40.

As mentioned above, no laboratory experiments are availlable to compare with, and the two-phase flow was simulated using water-wet conditions. However, the simulations can be performed for any desired wettability. This opens up the option to perform extensive wettability sensitivity studies, which is particularly valuable in absence of any knowledge about the wetting conditions.

CONCLUSIONS

The following are summarized results of a case study involving three carbonate reservoir core samples, comprising three vastly different reservoir rock types:

- The average formation porosity is obtained directly from MCT imaging and segmentation process, and the obtained values are consistent for all rock types within 15-20% range.
- Computed MCT models provided robust grid estimations of permeability and formation factors in three directions, and average properties at reservoir conditions. These are matched very closely to the measurements unless there is significant microporosity (micritic pores) which may in turn, invalidate the laboratory measurements. This is reflected in the comparatively poor match with Sample Sn-40.
- MCT-derived pore network models gave very good estimations of laboratory measured cementation exponent 'm', and saturation exponent 'n' during both primary drainage and first imbibition cycles. Primary drainage based Pc (such as MICP) results can also be generated through the technique.
- The capillary pressures obtained during the primary drainage and first imbibition cycles are modeled with a good degree of certainty.
- Assuming flow is driven by capillary pressure, fluids are immiscible and viscous forces are neglected, the *e-Core* technology allows rapid evaluation of reservoir condition water-oil relative permeability during primary drainage, first imbibition and secondary drainage cycles in carbonate reservoir cores. The technique is strongly influenced by assumed wettability conditions (pore geometry, contact angle and IFT) during the relative permeability tests, and hence can generate excellent scenarios for sensitivity studies to model the core scale reservoir behavior.
- Savings in costs and time, and more importantly robust predictions of two-phase flow behavior make the *e-Core* technology a viable alternative to conventional SCAL tests.

ACKNOWLEDGEMENTS

The authors wish to thank ADNOC and ADCO Management for permission to present the results of this case study. Special thanks to Maher Al Kenawy, Bruno Stenger and Ghaniya Bin-Dhaeer Al Yafei of ADCO for the contributions in the healthy discussions.

REFERENCES

1. Bakke, S. and Øren P.E., "3-D Pore-Scale Modeling of Sandstones and Flow Simulations in the Pore Networks", *SPEJ*, 1997, **2**, 136-149
2. Boller, E., “Experiment report: Microtomography tests on rocks”, ESRF, Grenoble, 2006.
3. Grotsch J., “Reservoir rock typing scheme for the Upper Thamama reservoirs”, ADCO internal report, June 1997.
4. Dong, H. and Blunt, M.J., “Pore-network extraction from micro-computerized-tomography images”, *Physical Review E*, **80** (3): 036307, 2009.
5. Lomeland, F., Ebeltoft, E., and Thomas, W. H., “A new versatile relative permeability correlation”, *Proceedings of the 2005 SCA Symposium*, Toronto, Canada, 21-25 August, 2005.
6. Øren, P.E. and Bakke, S., "Process Based Reconstruction of Sandstones and Prediction of Transport Properties", *Transport in Porous Media*, 2002, **46**, 311-343.
7. Øren, P.E., Bakke, S., and Arntzen, O.J., "Extending Predictive Capabilities to Network Models", *SPEJ*, December 1998, 324-336.
8. Skjæveland, S.M., Siqveland, L.M., Kjosavik, A., Hammervold Thomas, W.L., and Virnovsky, G.A., “Capillary Pressure Correlation for Mixed-Wet Reservoirs”, *SPE Reservoir Evaluation & Engineering*, 2000, **3** (1), 60-67.
9. Strohmenger, Christian J., L. Jim Weber, Ahmed Ghani, Khalil Al-Mehsin, Omar Al-Jeelani, Abdulla Al-Mansoori, Taha Al-Dayyani, Lee Vaughan, Sameer A. Khan, and John C. Mitchell. AAPG Special Publication Memoir 88. Giant Hydrocarbon Reservoirs of the World: From Rocks to Reservoir Characterization and Modeling edited by P. M. (Mitch) Harris and L. J. (Jim) Weber. Chapter 4: High-resolution Sequence Stratigraphy and Reservoir Characterization of Upper Thamama (Lower Cretaceous) Reservoirs of a Giant Abu Dhabi Oil Field, United Arab Emirates, 2006.

Table 1 : Input data for the flow simulations performed on the carbonate MCT models.

Water density	[kg/m^3]	1000
Oil density	[kg/m^3]	700
IFT_{WO}	[dynes/cm]	30
Receding contact angles		0-10

Table 2a: Sn-5 petrophysical properties calculated on the MCT model (*e-Core*) versus laboratory data (Lab; reservoir conditions). The average for the absolute permeability is arithmetic; the one for the formation factor is the harmonic mean. The laboratory porosity measurement is He-porosity.

Property/Sample	Sn-5	
	e-Core	Lab.
ϕ [%]	**18.82**	**26.8**
k_x [mD]	5706	
k_y [mD]	5555	
k_z [mD]	5114	
$k_{average}$ [mD]	**5114**	**5336**
FRF_x	23.5	
FRF_y	26.1	
FRF_z	28.7	
FRF_{avg}	**25.9**	**16.5**
m-exponent	**1.95**	**2.02**

Table 2b: Sn-5 resistivity index and end-state saturations calculated on the MCT model (*e-Core*) versus laboratory data (Lab; reservoir conditions).

Property/Sample	Sn-5	
	e-Core	Lab.
n-exponent D1	**1.78**	**2.12**
n-exponent Imb.	**2.04**	**2.28**
Swi	**0.03**	**0.08**
Sorw	**0.18**	**0.17**
krw@Sorw	**0.63**	**1.21**
Sw final after D2	**0.095**	**0.20**

Imb. = first imbibition, D1 = primary drainage, D2 = secondary drainage, Swi = irreducible water saturation, Sorw = residual oil saturation, krw@Sorw = water relative permeability at residual oil saturation.

Table 3a: Sn-34 petrophysical properties calculated on the MCT model (*e-Core*) versus laboratory data (Lab.; reservoir conditions). The average for the absolute permeability is arithmetic; the one for the formation factor is the harmonic mean. The laboratory porosity measurement is He-porosity.

Property/Sample	Sn-34	
	e-Core	Lab.
ϕ [%]	**26.48**	**22.6**
k_x [mD]	5.94	
k_y [mD]	7.24	
k_z [mD]	5.96	
$k_{average}$ [mD]	**5.96**	**2.92**
FRF_x	20.3	
FRF_y	18.6	
FRF_z	22.1	
FRF_{avg}	**20.2**	**19.45**
m-exponent	**2.22**	**2.32**

Table 3b: Sn-34 resistivity index and end-state saturations calculated on the MCT model (*e-Core*) versus laboratory data (Lab.; reservoir conditions).

Property/Sample	Sn-34	
	e-Core	Lab.
n-exponent D1	1.78	2.32
n-exponent Imb.	2.14	2.34
Swi	0.03	0.084
Sorw	0.11	0.14
krw@Sorw	0.83	1.22
Sw final after D2	0.05	0.08

Imb.= imbibition, D1 = primary drainage, D2= secondary drainage, Swi= irreducible water saturation, Sorw= residual oil saturation, krw@Sorw= water relative permeability at residual oil saturation.

Table 4a: Sn-40 petrophysical properties calculated on the MCT model (*e-Core*) versus laboratory data (Lab.; reservoir conditions). The average for the absolute permeability is arithmetic; the one for the formation factor is the harmonic mean. The laboratory porosity measurement is He-porosity.

Property/Sample	Sn-40	
	e-Core	Lab.
ϕ [%]	14.58	11.2
k_x [mD]	0.697	
k_y [mD]	0.357	
k_z [mD]	0.214	
$k_{average}$ [mD]	0.423	0.02
FRF_{avg}	172	67.05
m-exponent	1.98	1.89

Table 4b: Sn-40 resistivity index and end-state saturations calculated on the MCT model (*e-Core*) versus laboratory data (Lab.; reservoir conditions).

Property/Sample	Sn-40	
	e-Core	Lab.
n-exponent D1	3.3	1.41
n-exponent Imb.	2.36	1.62
Swi	0.17	0.12
Sorw	0.48	0.26
krw@Sorw	0.05	No data
Sw final after D2	0.18	No data

Imb.= imbibition, D1 = primary drainage, D2= secondary drainage, Swi= irreducible water saturation, Sorw= residual oil saturation, krw@Sorw= water relative permeability at residual oil saturation.

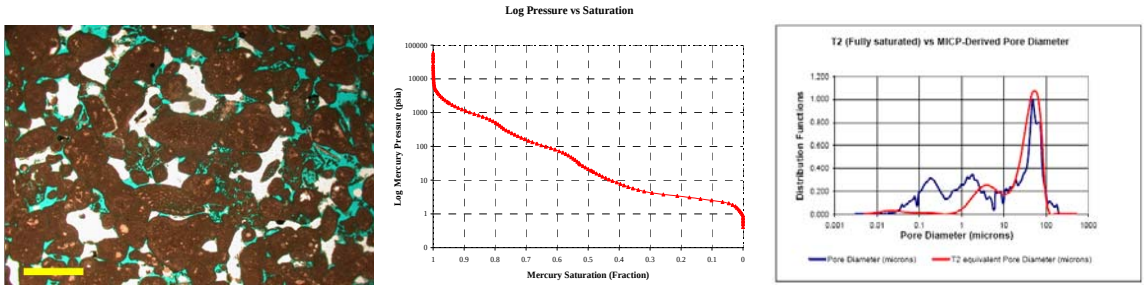

Figure 1: Left: thin section of sample Sn-5 (from MICP core plug "end trim") showing Coated-Grain, Skeletal Grain stone (CgSG; white and blue areas represent porosity; yellow scale bar is 500 µm). Middle: capillary pressure vs Hg saturation. Right: comparison of pore throat diameter from laboratory measurement (in blue) compared with NMR T2 pore throat diameter (in red).

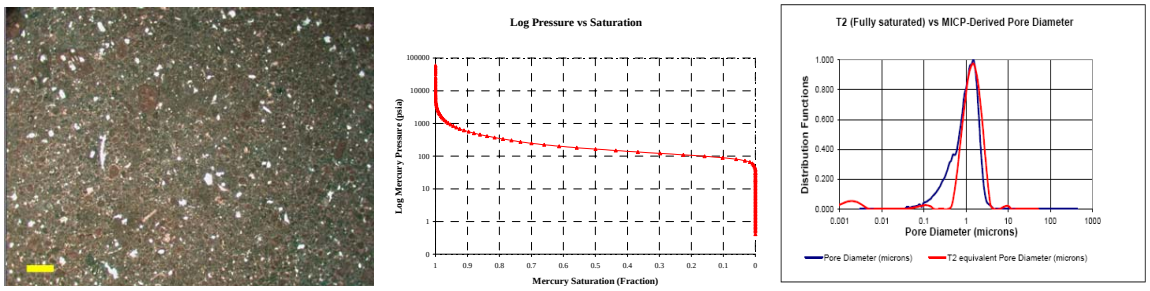

Figure 2: Left: thin section of sample Sn-34 (from MICP core plug "end trim") showing Skeletal, Peloid Packstone (SPP; white and blue areas represent porosity, yellow scale bar is 200µm). Middle: capillary pressure vs Hg saturation. Right: comparison of pore throat diameter from laboratory measurement (in blue) compared with NMR T2 pore throat diameter (in red).

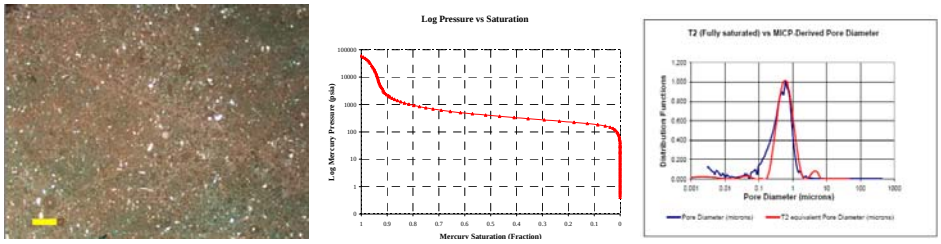

Figure 3: Left: thin section of sample Sn-40 (from MICP core plug "end trim") showing Skeletal, Peloid Wackestone-Packstone (SPWP; white and blue areas represent porosity, yellow scale bar is 250µm). Middle: capillary pressure vs Hg saturation. Right: comparison of pore throat diameter from laboratory measurement (in blue) compared with NMR T2 pore throat diameter (in red).

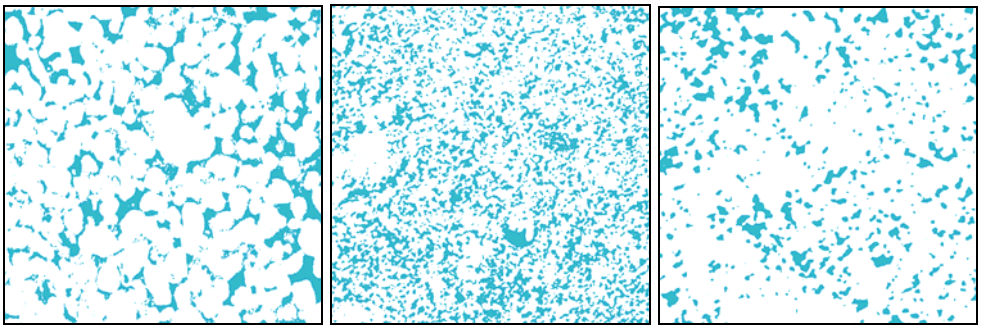

Figure 4: Two-dimensional slices of the 3D MCT images after pre-processing Sn-5 (left; image width = 6.65mm), Sn-34 (middle; image width = 280µm), Sn-40 (right; image width = 140µm). White color indicates carbonate grains and matrix, blue color represents pore space.

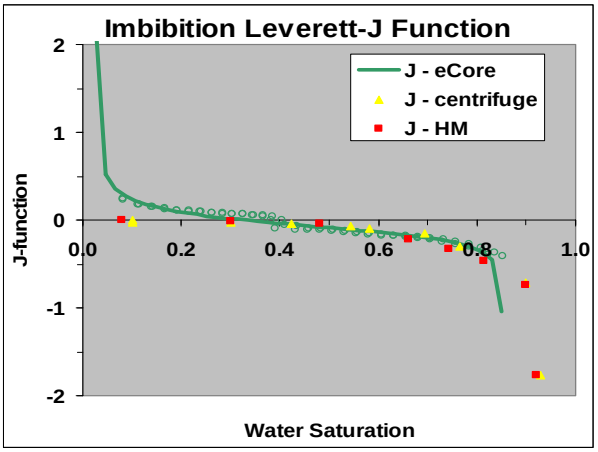

Figure 5: Sn-5 imbibition Leverett-J Function simulated on the MCT model (*e-Core*; green) versus laboratory data (HM: history matching in red; centrifuge data in yellow).

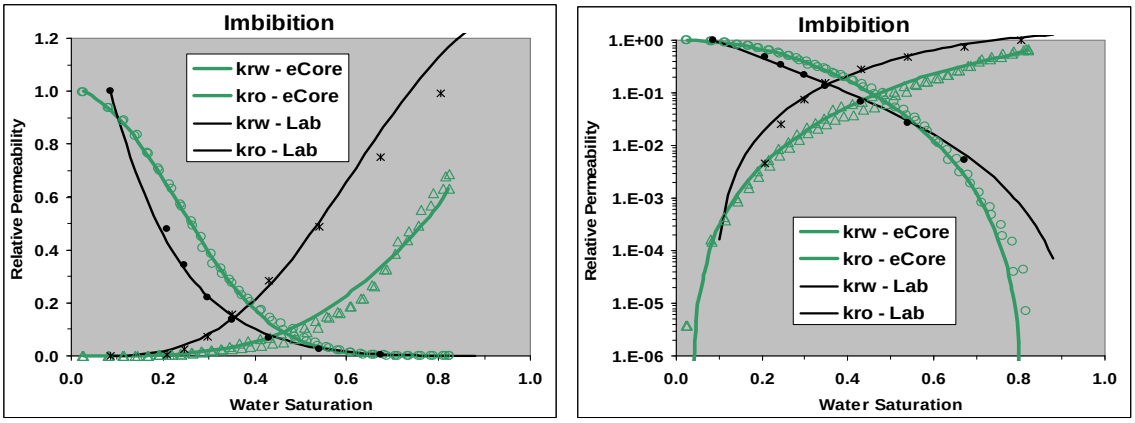

Figure 6a: Sn-5 imbibition relative permeability curves simulated on the MCT model (*e-Core*; green) versus laboratory data (Lab, reservoir conditions; black symbols are steady-state measurements, black line is Sendra data). Note that krw at Sorw for the laboratory measurements is larger than 1.

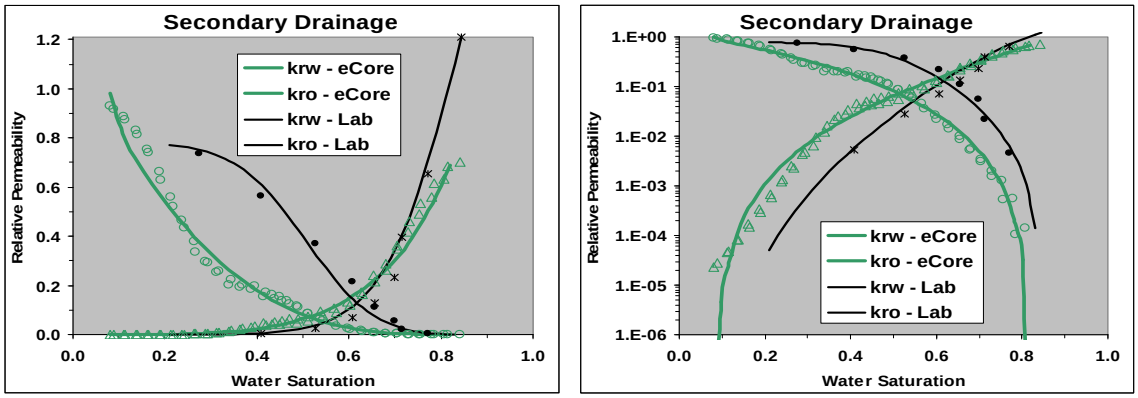

Figure 6b: Sn-5 secondary drainage relative permeability curves simulated on the MCT model (*e-Core*; green) versus laboratory data (Lab, reservoir conditions; black symbols are steady-state measurements, black line is Sendra data).

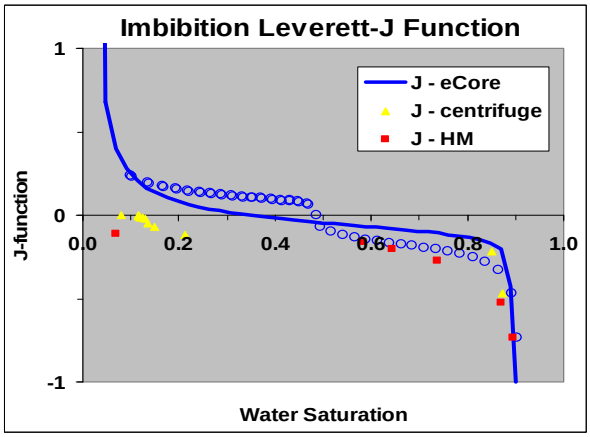

Figure 7a: Sn-34 imbibition Leverett-J Function simulated on the MCT model (*e-Core*; blue) versus laboratory data (HM: history matching in red; centrifuge in yellow).

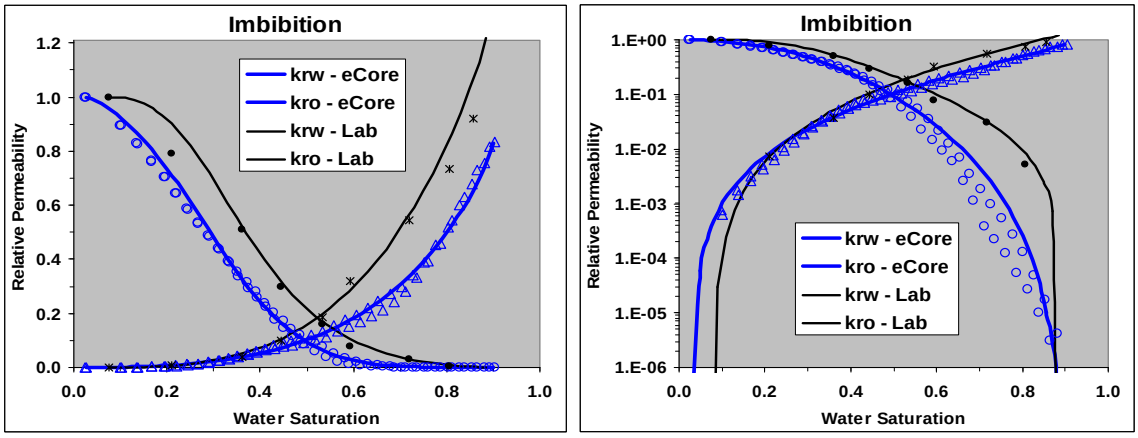

Figure 7b: Sn-34 imbibition relative permeability curves simulated on the MCT model (*e-Core*; blue) versus laboratory data (Lab, reservoir conditions; black symbols are steady-state measurements, black line is Sendra data). Note that krw at Sorw for the laboratory measurements is larger than 1.

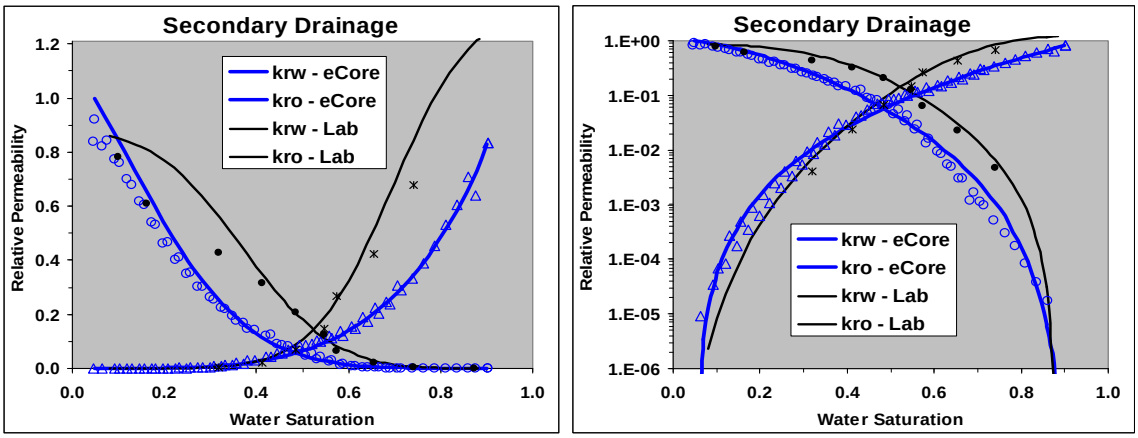

Figure 7c: Sn-34 secondary drainage relative permeability curves simulated on the MCT model (*e-Core*; blue) versus laboratory data (Lab, reservoir conditions; black symbols are steady-state measurements, black line is Sendra data).

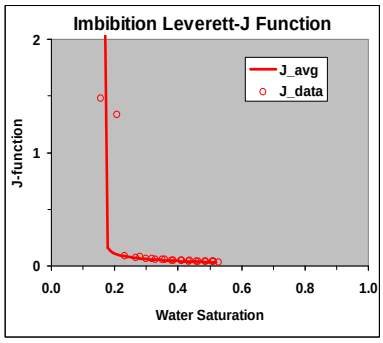

Figure 8a: Imbibition Leverett-J Function simulated on the MCT model of sample Sn40.

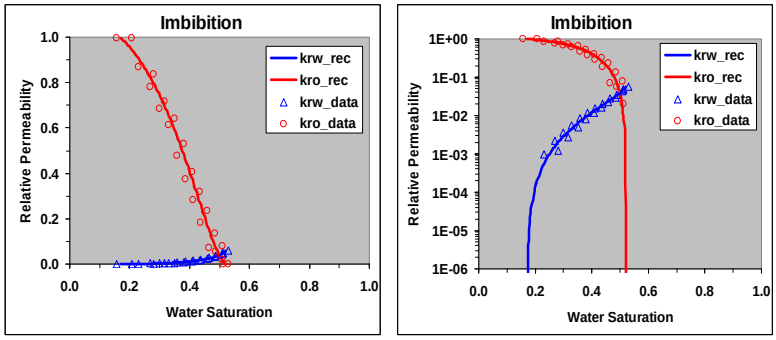

Figure 8b: Imbibition relative permeability curves simulated on the MCT model of sample Sn40

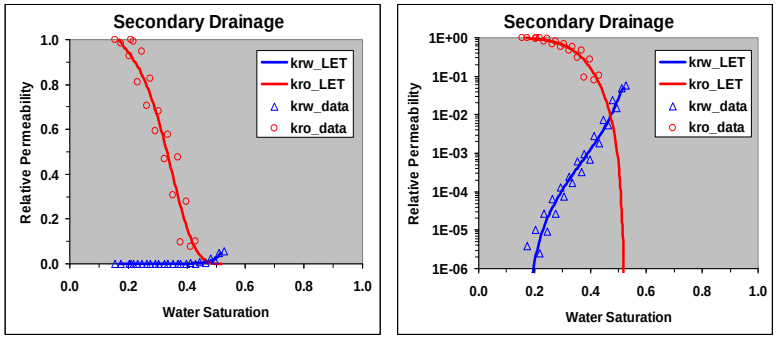

Figure 8c: Secondary drainage relative permeability curves simulated on the MCT model of sample Sn-40.